Resonant soft-x-ray emission study in relation to the band structure of *c*BN

A. Agui, S. Shin, M. Fujisawa, Y. Tezuka, and T. Ishii
Synchrotron Radiation Laboratory, Institute of Solid State Physics, University of Tokyo, 3-2-1 Midori-cho, Tanashi-shi, Tokyo 188, Japan

Y. Muramatsu
NTT Integrated Information & Energy Systems Laboratories, 3-9-11, Midori-cho, Musashino-shi, Tokyo 180, Japan

O. Mishima and K. Era*
National Institute for Research in Inorganic Materials, 1-1 Namiki, Tsukuba-shi, Ibaraki 305, Japan
(Received 10 January 1996; revised manuscript received 3 September 1996)

The resonant soft-x-ray emission (SXE) and its total photon yield (TPY) spectra were measured at the B 1*s* and N 1*s* edges of cubic boron nitride (*c*BN) using undulator radiation. The band-gap energy was found to be about 6.2 eV, which is in good agreement with other experiments. It was found that the emission from the high symmetry point in the SXE spectrum is enhanced when the same high symmetry point in the TPY spectrum is excited. The line shapes in both the SXE and N 1*s* TPY spectra were consistent with the calculated partial density of states, though the total bandwidth was not well reproduced. On the other hand, the exciton effect was found to be strong in the B 1*s* TPY spectra. [S0163- 1829(97)08704-3]

I. INTRODUCTION

Soft-x-ray absorption and emission spectroscopies (SXES) have been used to study the electronic properties of matters for a long time. Recently, SXES studies have been performed by means of the inelastic-light-scattering process using high-brilliance synchrotron radiation as an excitation light source.[1–8] Using synchrotron radiation, one can utilize the excitation energy dependence of the SXES, which provides an experimental method to understand the electronic structure of matters in relation to the band structure.

Since the soft x ray has a longer mean free path in matter than the electron does, the SXE technique has several advantages including sensitivity to bulk characteristics. The SXE spectra can be measured without the problem of sample charging, which happens in photoemission measurements. The SXE spectra reflect the partial density of states (PDOS), since the emission process is caused by the dipole transition. Furthermore, the spectral features characteristics of specific atomic species arise, because the core hole is strongly localized.

Very recently, it was found that the SXE process from the valence band is enhanced at the high symmetry point, where the same symmetry as the conduction band was excited.[1–7] This is the resonant fluorescence or the inelastic light-scattering process, where the wave vector of the valence hole is the same as that of the excited electron. Thus, momentum-resolved inelastic light scattering offers a band mapping technique.[2,5]

In this study, we used cubic boron nitride (*c*BN) to measure boron 1*s* (B 1*s*) and nitrogen 1*s* (N 1*s*) SXES and their total photon yield (TPY) spectra. Cubic BN is the simplest III-V semiconductor. The crystal structure of *c*BN is the zinc-blend type, which is isostructural to the diamond. Since *c*BN has several interesting physical properties, such as a wide band gap, extreme hardness, and a high melting point, the electronic structure of *c*BN has been studied by optical reflectivity, absorption, x-ray emission spectroscopy,[9–15] and photoemission spectroscopy.[33] Many theoretical band calculations have been carried out,[16–30] because of its simple crystal structure and small number of electrons. However, the correspondence between the theoretical calculation and the experiment has not been so good. An indirect gap of about 6.2 eV was found by ultraviolet reflectivity spectroscopy.[12,13] Recently, a weak core exciton (CE) has been found in *c*BN by photoelectron spectroscopy,[33] although hexagonal-type BN (hBN) has intense core excitons.[31,32]

The aim of the present study is to investigate the resonant B 1*s* and N 1*s* SXE processes in relation to the electronic structure of *c*BN for B 1*s* and N 1*s* excitation edges. The B 1*s* SXES has been carried out on several boron compounds such as B_2O_3 (Refs. 6, 34, and 35) and *h*BN.[31,32] Cubic BN is one of the most suitable materials to study the relation between the band structure and the soft x-ray inelastic-light-scattering process, because *c*BN has the simplest band structure among boron compounds. Results of this work suggest that inelastic light scattering will be a powerful technique to investigate the site-projected band mapping even in multiternary materials.

Since the B 1*s* and N 1*s* core states have flat band dispersions, the SXES spectra reflect the valence-band PDOS, and the TPY spectra reflect the conduction-band PDOS. It is said that the TPY spectrum corresponds to the absorption spectra. The 1*s* SXE and TPY spectra reflect only the 2*p* character in the valence and conduction band, respectively, while the photoemission spectroscopy (PES) spectrum is similar to the total DOS curve, considering the cross sections of atomic components, B 2*s*, B 2*p*, N 2*s*, and N 2*p*, because they are governed by the dipole selection rules.

II. EXPERIMENT

The experimental measurements of *c*BN were performed on two undulator beam lines, BL-2B and BL-19B of the

Photon Factory (PF) located at the National Laboratory for High Energy Physics (KEK). Synchrotron radiation was monochromatized by a Vorder-type 10-m grazing incidence monochromator at BL-2B.[36] A variable-spacing plane grating monochromator without an entrance slit was used at BL-19B.[37] Data collection time was typically 0.5 h for B 1*s* SXES at BL-19B and 2 h for N 1*s* SXES at BL-2B.

The B 1*s* SXES were measured at a temperature below 30 K in order to suppress the photon effect, using a closed-cycle He refrigerator. The base pressure of the analyzer chamber was about 3×10^{-11} Torr.

The *c*BN single crystal was synthesized by the temperature-difference method at around 2000 K and under high pressures around 5 GPa in a small molybdenum crucible using a flux or catalytic solvent of $LiCaBN_2$ or Li_3BN_2.[38] The typical size of the crystal was about 2×2 mm^2.

The SXE spectrometer[39] consists of an input slit, a spherical grating, and a CsI-coated microchannel detector. They are placed on a Rowland circle so that the detector is controlled by three-axes movement. The TPY was measured by collecting all SXE above 4 eV emitted from the sample.

The photon energy calibration of the beam line monochromator and SXE spectrometer is very important. The PES and the SXES can be measured at the same time in this experimental system.[37] The photon energy of the beamline monochromator was calibrated by PES of the Fermi edge or 4*f* level of gold on the sample holder. The photon energy of the SXE spectrometer was calibrated by measuring the reflection light of the same light that was used in the PES measurement.

III. RESULTS AND DISCUSSIONS

A. Band structure of *c*BN

Figure 1 shows (a) B 1*s* SXE and TPY spectra and (b) N 1*s* SXE and TPY spectra, in comparison with (c) the calculated band dispersion curve[28] of *c*BN. The dots in Fig. 1(a) show the TPY spectrum and two B 1*s* SXE spectra of *c*BN, which were measured at the photon excitation energies $h\nu_e$=220.75 eV (No. 25) and 194.16 eV (No. 1). Features in the B 1*s* SXES are designated with letters *A* to *H*. The vertical bars in the TPY spectrum, which are numbered from 1 to 25, indicate the selected excitation photon energies for the resonant B 1*s* SXES measurements.

The solid lines in Fig. 1(a) show the PDOS of B 2*p* component, which were calculated by Xu and Ching.[28] Considering the dipole selection rule of SXES, B 1*s* SXES has to be compared with the B 2*p* PDOS curve. The dashed lines show the B 2*p* PDOS convoluted with the Lorentzian and the Gaussian functions whose widths correspond to the lifetime broadening and the experimental resolution, respectively. The full widths at half maximum (FWHM) of the Gaussians are 1 and 0.05 eV for the valence band and the conduction band, respectively. The FWHM of the Lorentzian functions are $(0.1+0.1|E_B|)$ eV and $(0.1+0.1|E_B-6.2|)$ eV for the valence and the conduction bands, respectively.

The correspondence between the energy positions of the band calculation and the experimental spectra is not so good. In particular, the calculated total bandwidth is too narrow. Also, the calculated band gap is too narrow. The calculated

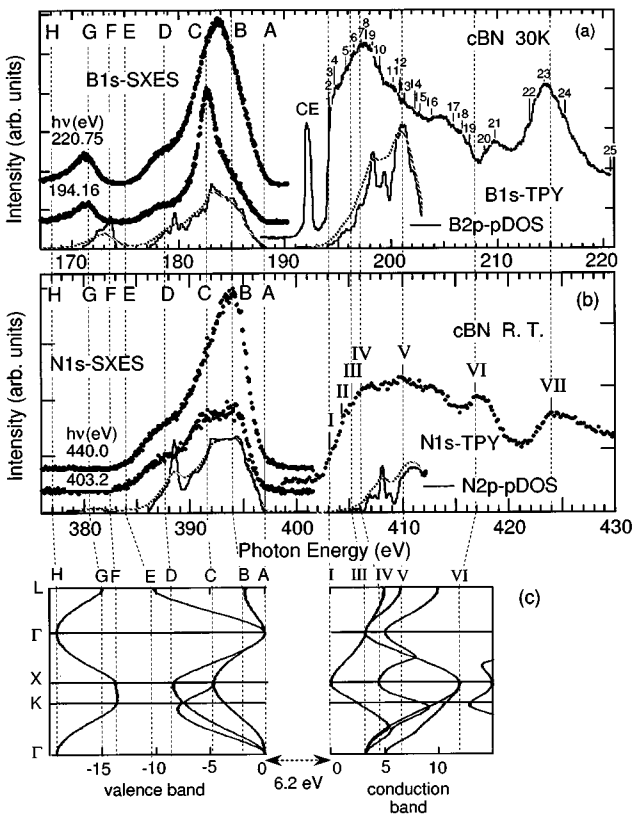

FIG. 1. (a) Dots show the B 1*s* SXE and its TPY spectra of *c*BN. The spectra are measured with the excitation energy $h\nu_e$=220.75 and 194.16 eV, respectively. The solid line is an example of the calculated B 2*p* PDOS (Ref. 28). The dashed line shows the convoluted B 2*p* PDOS curves with Lorentzian and the Gaussian functions. The CE means the core exciton. (b) Dots show the N 1*s* SXE and its TPY spectra of *c*BN. The spectra measured with the excitation energy $h\nu_e$=440.0 and 403.2 eV, respectively. The solid line is an example of the calculated N 2*p* PDOS (Ref. 28). The dashed line shows the convoluted N 2*p* PDOS curves. (c) The band dispersion curve of *c*BN calculated by Xu and Ching (Ref. 28).

bandwidth can be in good agreement with the experimentally observed width if it is expanded by a factor of about 1.12. Here, in order to compare with the spectra, the energy position of the calculated spectrum of the filled states is shifted to fit the top of the valence band of the SXES in Fig. 1(a). On the other hand, the calculated density of empty states is shifted to fit the bottom of the conduction band of the TPY spectrum. It is difficult to determine the location of the top of the valence band or the bottom of the conduction band exactly. Here, we determined their locations within the uncertainties of the resolution.

The prominent B 1*s* SXES structures *B* ($h\nu_{\mathrm{SXE}}$ =185 eV) and *G* (171.5 eV) and a shoulder *D* (178.6 eV) were found in Fig. 1(a), where $h\nu_{\mathrm{SXE}}$ represents the photon energy of SXE. The main features of the experimental spectrum that was measured at 25 ($h\nu_e$=220.75 eV) were reproduced by the PDOS calculation, though the energy position of structure *G* was not in good agreement. The spectrum at 25 ($h\nu_e$=220.75 eV) corresponds to the fluorescence spectrum, so that its line shape becomes similar to the B 1*s* PDOS curve. The structure *C* ($h\nu_{\mathrm{SXE}}$=187.6 eV) is much stronger

in the spectrum that was measured around the lowest conduction band at 1 ($h\nu_e$=194.16 eV).

On the other hand, the features of the TPY spectrum are quite different from the calculation. A sharp structure (CE) was found around $h\nu_e$=192 eV in the B 1*s* TPY spectrum in Fig. 1(a). Because this structure is located below the other conduction band and was not observed in the band calculation, the structure was assigned to be the core-exciton structure. The core exciton has been already observed by Fomichev *et al.*[9] in TPY and by Shin *et al.* in the total electron yield (TEY) spectra.[33] Shin *et al.* measured the resonant PES and CIS (constant initial state) spectra around CE region, and found the strong resonance enhancement of the valence band structure at the CE structure. This fact also suggests that the CE is a core exciton structure. However, the intensity of the CE structure in this experiment is much higher and its width is much sharper than that observed by Fomichev *et al.* and Shin *et al.* Its intensity has a strong incidence angle dependence, which will be discussed in a separate paper.[40] Furthermore, the calculated DOS curve at the conduction-band minimum was not well reproduced by the band calculation. The spectrum had a clear band edge at the conduction-band minimum, while the calculated B 2*p* PDOS curve increases gradually. The difference between the DOS curve and the TPY spectrum was also ascribed to core exciton effects. One could consider the core exciton structure of *c*BN as a Wannier-type exciton. That is, the CE and the features around 1 may be assigned to be 1*s* and 2*s* structures of the Wannier-type exciton.

Figure 1(b) shows the TPY spectrum and two N 1*s* SXE spectra, which were measured at $h\nu_e$=440 eV and 403.2 eV (No. I) of *c*BN. The dotted spectra are the experimental data and the solid lines are the calculated N 2*p* PDOS curve.[28] The dashed line shows the N 2*p* PDOS convoluted with Lorentzian and Gaussian functions. The widths of Gaussians that correspond to the resolution of SXES and TPY were about 1.5 and 0.1 eV, respectively. The linewidths of the Lorentzian are the same as in the case of B 2*p* PDOS. The energy positions of both calculated conduction and valence bands were shifted in the same way as for Fig. 1(a). Features in N 1*s* SXES were designated with letters from *A* to *H* whose energy positions are the same as those in B 1*s* SXES. The several photon energies, which are numbered I to VII on the N 1*s* TPY spectrum, were selected to examine the excitation energy dependence of the N 1*s* SXES.

A prominent spectral feature was found at *B* ($h\nu_{\mathrm{SXE}}$ =394 eV), and a shoulder at *D* (387.6 eV) in Fig. 1(b). The lower valence band around *G* ($h\nu_{\mathrm{SXE}}$=381.6 eV), which is weak in the calculated spectrum, is very weak in the SXE spectrum. The SXES spectrum measured at $h\nu_e$=440 eV is well in accord with the N 2*p* PDOS curve, while the structure *C* ($h\nu_{\mathrm{SXE}}$=391.6 eV) is emphasized for that measured at I ($h\nu_e$=403.2 eV). This photon-energy dependence is very similar to that in B 1*s* SXES.

The spectral features of experimental N 1*s* TPY are reproducible by the calculated conduction-band structure, though those of B 1*s* TPY are different from the calculation. No CE structure is observed in the N 1*s* TPY spectrum. This fact shows that the conduction-band minimum mainly consists of the B 2*p* component and the contribution from N 2*p* is small.

TABLE I. Measured band gap and bandwidths of *c*BN. VB represents valence band.

Band gap		6.2 eV
Bandwidths	Upper VB	13.0 eV
	Lower VB	5.5 eV
	Total VB	20 eV

It is clear from these SXES measurements that the upper valence bands from *A* to *E* structures are mainly composed of both B 2*p* and N 2*p* components. This fact is consistent with the band calculations.[26] The main structures *C* on B 1*s* and N 1*s* SXES are due to the substantial orbital hybridization between B 2*p* and N 2*p* states. The band calculation suggests that the lower valence bands from *E* to *H* structures are mainly composed of N 2*s* components. In fact, N 1*s* SXES shows that the N 2*p* PDOS is negligible and B 1*s* SXES shows that the B 2*p* PDOS is rather strong in the lower valence bands. The B 2*p* components are mixed across the whole valence band, while the N 2*p* and N 2*s* bands are localized in upper and lower valence bands, respectively.

Because SXE and TPY spectra are plotted with the same abscissa, one can find that the band gap between the valence and conduction band is about 6.2 eV, if we neglect the sharp CE structure. This value is consistent with other experimental results. However, the band calculations, which were carried out by means of local density approximation (LDA) and other methods, indicate smaller band gaps.[27–36] On the other hand, a quasiparticle band calculation is in good agreement with our result. The *c*BN band gap and valence bandwidths obtained by the present study are listed in Table I.

B. Excitation energy dependence of SXE spectra

Figure 2(a) shows the B 1*s* SXE spectra of *c*BN, which are excited at various photon energies. The intensities of SXES are normalized by the excitation photon intensity and data collection time. The selected excitation energies are indicated by the numbers in the TPY spectrum in Fig. 1(a). The spectra have a clear excitation energy dependence. The SXE spectrum measured around the conduction band minimum 1 has a rather sharp peak *C*. The top of the valence-band increase at the SXE spectrum measured at 10 ($h\nu_e$=198.99 eV). The SXE spectra do not show any prominent photon energy dependence at photon energies higher than $h\nu_e$=220.75 eV (not shown), where the fluorescence component seems to be dominant compared with the inelastic light scattering component.

Figure 2(b) shows the difference spectra where each spectrum of Fig. 2(a) is subtracted by the factored $h\nu_e$ =220.75 eV spectrum. The multiplying factors are shown by the figures in the parentheses. We determine the factors so that the difference spectrum enhances the excitation-energy dependence. Since the $h\nu_e$=220.75 eV spectrum is thought to be the fluorescence spectrum, the differences mainly correspond to the inelastic-light-scattering spectra. In Fig. 2(b), a sharp structure *C* is enhanced by the excitation at 1 ($h\nu_e$=194.16 eV), 8 (197.75 eV), 17 (205.88 eV), 19 (207.42 eV), and 23 (214.48 eV). A broad structure around *B* is enhanced at 13 ($h\nu_e$=201.25 eV) and 22 (213.06 eV).

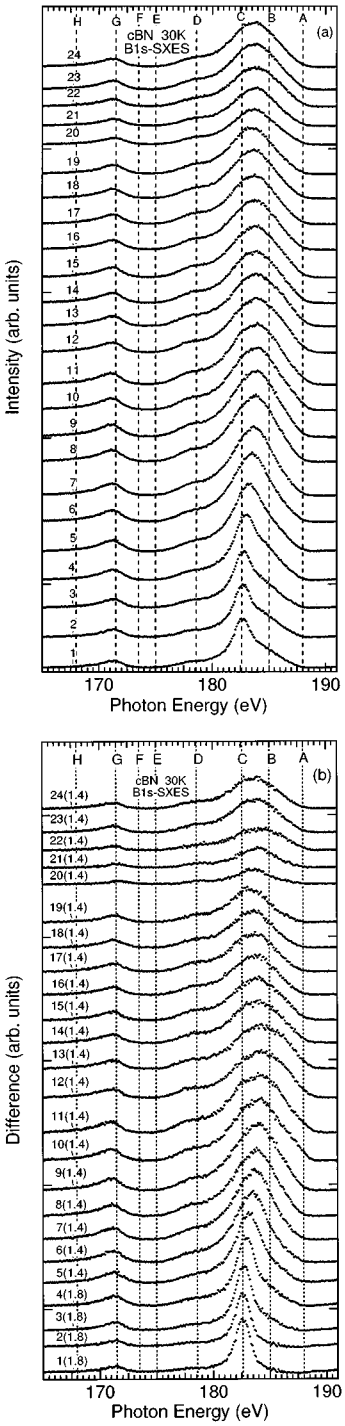

FIG. 2. (a) The B 1*s* SXE spectra excited at various photon energies numbered in Fig. 1(a), which are indicated on the left-hand sides of the spectra. (b) Difference spectra that were subtracted by the spectrum measured at $h\nu_e$=220.75 eV. The multiplying factors of the $h\nu_e$=220.75 eV spectrum are shown in the parentheses.

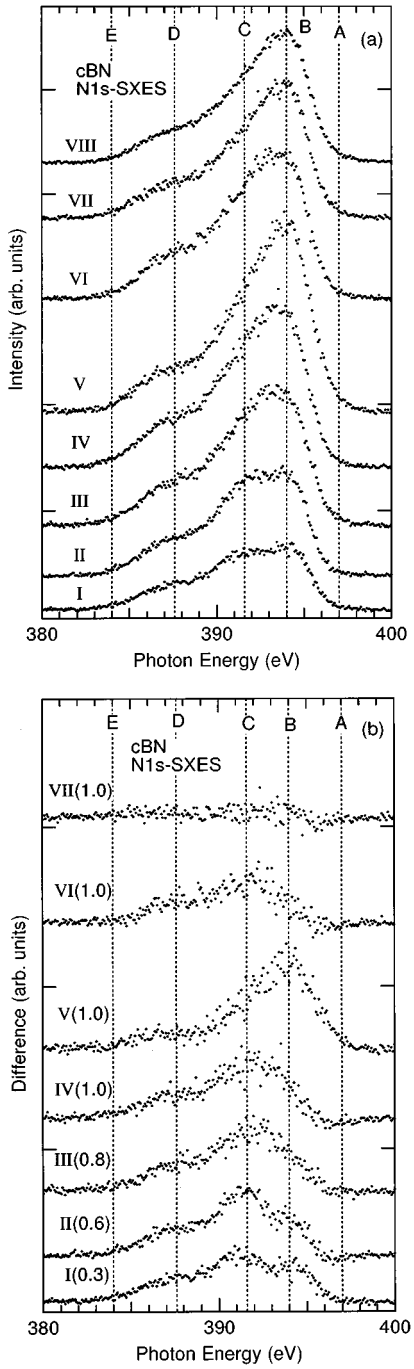

FIG. 3. (a) The N 1*s* SXE spectra excited at various photon energies numbered in Fig. 1(b), which are indicated on the left-hand sides of the each spectra. (b) Difference spectra that were subtracted by the spectrum measured at $h\nu_e$=440.0 eV. The multiplying factors of the $h\nu_e$=440.0 eV spectrum are shown in the parentheses.

The N 1*s* SXE spectra in Fig. 3(a) were measured by the various photon energies indicated by the numbers in Fig. 1(b). Figure 3(b) shows the difference spectra obtained by subtracting the VIII ($h\nu_e$=440.0 eV) spectrum from each spectrum in Fig. 3(a). Since the excited photon energy at VIII is high above the N 1*s* threshold by about 37 eV, it is thought to be the fluorescence spectrum as in the case of B 1*s* SXES spectra. The spectra excited at I ($h\nu_e$=403.2 eV), II (404.3 eV), and III (405.2 eV) were subtracted by the VIII spectrum multiplied by 0.3, 0.6, and 0.8, respectively. In Fig. 3(b), structures at *C* and *D* are enhanced by the excitation at I, IV, and VI. A sharp SXES structure at *B* is enhanced by the excitation at V ($h\nu_e$=410.0 eV). A small hump at *A* is enhanced by the excitation at III.

Figure 1(c) is an example of the calculated band dispersion curves.[28] The high symmetry points are designated by the letters and numbers in Fig. 1(a) and Fig. 1(b). In Fig. 1(c), dashed lines *C* and *D* correspond to the high-symmetry

TABLE II. The relative energies from the valence-band maximum. The calculated energies are taken from Ref. 30. All energies are in eV.

	B 1s SXES		N 1s SXES		GW	
Assignment	No.	Relative	No.	Relative	Calculation	Component
X^C	23	26.5				
L^C	22	25.1				
X^C	21	21.8				
X^C	19	19.4	VI	19.8		
X^C	17	17.9				
L_3^C	13	13.3				
L_1^C	12	12.8	V	13.0	12.4	
Γ_1^C	10	11			12.6	
X_3^C	8	9.8	IV	9.1	11.3	
Γ_{15}^C	6	8.2	III	8.2	11.4	
X_1^C	1	6.2	I	6.2	6.3	B 2p dominant
Γ_{15}^V	A	0	A	0	0	B 2p dominant
L_3^V	B	−3.0	B	−3	−2.2	N 2p dominant
X_5^V	C	−5.4	C	−5.4	−5.5	B 2p dominant
X_3^V	D	−9.4	D	−9.4	−10.2	
L_1^V	E	−13.0	E	−13	−12.2	
X_1^V	F	−14.5			−16.9	
L_1^V	G	−16.5			−18.5	N 2s dominant
Γ_1^V	H	−20.0			−23.1	

X_5^V and X_3^V points, and the structures B and G correspond to the L_3^V and L_1^V points in the band calculation. The top of the valence band A corresponds to the Γ_{15}^V point.

The experimental results show that the energy positions of high symmetry points are consistent with each other in B 1s and N 1s SXE spectra. The intensity ratio of each structure is different, because the composition of N 2p and B 2p components is different. That is, the Γ_{15}^V and X_5^V bands have a stronger B 2p component than N 2p component. The main component of the L_3^V band is N 2p.

On the other hand, structures 1 and 8 in the B 1s TPY spectra correspond to X_1^C and X_3^C points, and structures near 12 and 13 consist mainly of emission from the L_1^C and L_3^C points. Structures at 6 and 10 are related to the Γ_{15}^C and Γ_1^C points, where Γ_1^C is indistinguishable from the L_1^C point. In the case of the N 1s TPY spectrum, the structures labeled I, III, IV, and V correspond to the high symmetry X_1^C, Γ_{15}^C, X_3^C, and Γ_1^C points.

It is clear that the feature C at the symmetry point X_5^V becomes evident when the core electron is excited to the X_1^C point at 1. Similarly, when the L_3^C point is excited, a valence hole is created preferentially at the L_3^V point to keep momentum conservation. Similar enhancement was found in the emission spectrum in the region of the X_3^V point. At the excitation energies around 17, the emission from the X_5^V point C is enhanced again. One can find that high symmetry points of the valence bands become prominent, when the electron is excited to the same symmetry in the conduction band. Recently, Ma *et al.* fond the similar excitation-photon-energy dependence in C 1s SXES of diamond.[2,5] They elucidated the excitation energy dependence in the SXES spectra by the inelastic-light-scattering process rather than the normal fluorescent process. In this process, the wave vectors of the excitation electron and the created core hole become the same. It was also found in this study that each atomic component in the compound has a photon energy dependence by the momentum conservation.

The PDOS calculation of the conduction band was carried out only up to 5 eV above the conduction-band minimum. By using SXES enhancement from an inelastic-light-scattering process, one can determine the high symmetry at higher energies without knowing the band calculations. In the case of B 2p PDOS, structures 17, 19, 21, 22, and 23 correspond to the high symmetry X^C, X^C, X^C, L^C, and X^C points, respectively.

The vacuum ultraviolet reflectance spectra was measured.[9] The assignments for high symmetry points are consistent with our results. The energy positions obtained are tabulated in Table II in comparison with the recent GW band calculations.[30] For the LDA, the bandwidths were too narrow compared with our experimental result. It was also found that calculation by the GW approximation accounts for the magnitude of the band gap. However, the GW approximation shows much greater bandwidth. Surh, Louie, and Cohen[30] pointed out that they cannot determine the other high symmetry points because there had been no experimental data available for the band calculation. Here, using an inelastic-light-scattering technique, we can find the high symmetry points without theoretical calculations. Detailed band calculations that reproduce the experimental results will be needed.

IV. CONCLUSION

The B 1s and N 1s SXES studies of cBN have been carried out. The line shapes of the calculated B 2p and N

$2p$ PDOS in the valence band are in good agreement with both experimental SXE spectra. The total bandwidth of the band calculation is much narrower than the experimental results. However, the calculated B $2p$ PDOS of the conduction band is very different from the B $1s$ TPY spectrum. The intense core-exciton structure was found in the B $1s$ TPY spectrum while it was not found in the N $1s$ TPY spectrum. We observed that the line shapes change in B $1s$ and N $1s$ SXES of *c*BN as the photon energy varies. The resonance enhancements are due to the momentum-conserved inelastic-light-scattering process. It was found that the inelastic-light-scattering method is a powerful tool to investigate the site-projected DOS in the compounds.

ACKNOWLEDGMENTS

This work was supported by grants-in-aid for Scientific Research the Ministry of Education, Science and Culture of Japan. The authors would like to thank Professors E. Hanamura, K. Terakura, and K. Nasu for their helpful discussions. Appreciation is due to Professor A. Yagishita and Dr. E. Shigemasa for their excellent suport.

*Present address: 1-13-12 Sengen, Tsukuba-shi, Ibaraki, 305, Japan.

[1] J-E. Rubensson, D. Mueller, R. Shuker, D. L. Ederer, C. H. Zhang, J. Jia, and T. A. Callcott, Phys. Rev. Lett. **64**, 1047 (1990).
[2] Y. Ma, N. Wassdahl, P. Skytt, J. Guo, J. Nordgren, P. D. Johnson, J-E. Rubensson, T. Boske, W. Eberhardt, and S. D. Keven, Phys. Rev. Lett. **69**, 2598 (1992).
[3] W. L. O'Brien, J. Jia, Q-Y. Dong, T. A. Callott, K. E. Miyano, D. L. Ederer, D. R. Mueller, and C-C. Kao, Phys. Rev. Lett. **70**, 238 (1993).
[4] Y. Ma, P. Skytt, N. Wassdahl, P. Glans, D. C. Mancini, J. Guo, and J. Nordgren, Phys. Rev. Lett. **71**, 3725 (1993).
[5] P. D. Johnson and Y. Ma, Phys. Rev. B **49**, 5024 (1994).
[6] Y. Muramatsu, M. Oshima, and H. Kato, Phys. Rev. Lett. **71**, 448 (1993).
[7] S. Shin, A. Agui, M. Watanabe, M. Fujisawa, Y. Tezuka, and T. Ishi, Phys. Rev. B **53**, 15 660 (1996).
[8] Y. Tezuka, S. Shin, A. Agui, M. Fujisawa, and T. Ishi, J. Phys. Soc. Jpn. **65**, 312 (1996).
[9] V. A. Fomichev and M. A. Rumsh, J. Phys. Chem. Solids **29**, 1015 (1968).
[10] R. M. Chrenko, Solid State Commun. **14**, 511 (1974).
[11] P. J. Gielisse, S. S. Mitra, J. N. Plendl, R. D. Griffis, L. C. Mansur, R. Marshall, and E. A. Pascoe, Phys. Rev. **115**, 155 (1967).
[12] N. Miyata, K. Moriki, O. Mishima, M. Fujisawa, and T. Hattori, Phys. Rev. B **40**, 12 028 (1989).
[13] A. Chayahara, H. Yokoyama, T. Imura, Y. Osaka, and M. Fujisawa, Jpn. J. Appl. Phys. **27**, 440 (1988).
[14] H. Yokoyama, M. Okamoto, T. Hamada, T. Imura, Y. Osaka, A. Chayahara, and M. Fujisawa, Jpn. J. Appl. Phys. **28**, 555 (1989).
[15] A. Onodera, M. Nakatani, M. Kobayashi, Y. Nisida, and O. Mishima, Phys. Rev. B **48**, 2777 (1993).
[16] L. Kleinman and J. C. Phillips, Phys. Rev. **117**, 460 (1960).
[17] D. R. Wiff and J. Keown, J. Chem. Phys. **47**, 3113 (1967).
[18] J. C. Phillips, J. Chem. Phys. **48**, 5740 (1968).
[19] L. A. Hemstreet, Jr. and C. Y. Fong, Phys. Rev. B **6**, 1464 (1972).
[20] A. Zunger and A. J. Freeman, Phys. Rev. B **17**, 2030 (1978).
[21] H-C. Hwang and J. Henkel, Phys. Rev. B **17**, 4100 (1978).
[22] Y. F. Tsay, A. Vaidyanathan, and S. S. Mitra, Phys. Rev. B **19**, 5422 (1979).
[23] R. Dovesi, C. Pisani, C. Roetti, and P. Dellarole, Phys. Rev. B **24**, 4170 (1981).
[24] C. Prasad and J. D. Dubey, Phys. Status Solidi B **125**, 629 (1984).
[25] R. M. Wentzcovitch, K. J. Chang, and M. L. Choen, Phys. Rev. B **34**, 1071 (1986).
[26] K. T. Park, K. Terakura, and N. Hamada, J. Phys. C **20**, 1241 (1987).
[27] E. K. Takahashi, A. T. Lino, A. C. Ferraz, and J. R. Leite, Phys. Rev. B **41**, 1691 (1990).
[28] Y-N. Xu and W. Y. Ching, Phys. Rev. B **44**, 7787 (1991).
[29] K. Kikuchi, T. Uda, A. Sakuma, M. Hirao, and Y. Murayama, Solid State Commun. **81**, 653 (1992).
[30] M. P. Surh, S. G. Louie, and M. L. Cohen, Phys. Rev. B **43**, 9126 (1991).
[31] J. Barth, Kunz, and T. M. Zimkina, Solid State Commun. **36**, 456 (1980).
[32] B. M. Davies, F. Bassani, F. C. Brown, and C. G. Olson, Phys. Rev. B **24**, 3537 (1981).
[33] S. Shin, A. Agui, M. Fujisawa, T. Ishii, Y. Minagawa, Y. Suda, A. Ebina, O. Mishima, and K. Era, Phys. Rev. B **52**, 11 853 (1995).
[34] F. V. Broen, R. G. Bacharack, and M. Skibowski, Phys. Rev. B **13**, 3633 (1977).
[35] R. D. Carson and S. E. Schnatterly, Phys. Rev. Lett **59**, 319 (1987).
[36] A. Yagishita, S. Masui, T. Toyoshima, H. Maezawa, and E. Shigemasa, Rev. Sci. Instrum. **63**, 1351 (1991).
[37] M. Fujisawa, A. Harasawa, A. Agui, M. Watanabe, A. Kakizaki, S. Shin, T. Ishii, T. Kita, T. Harada, Y. Saitoh, and S. Suga, Rev. Sci. Instrum. **67**, 345 (1996).
[38] O. Mishima, S. Yamaoka, and O. Fukunaga, J. Appl. Phys. **61**, 2822 (1987).
[39] S. Shin, A. Agui, M. Fujisawa, Y. Tezuka, T. Ishii, and N. Hirai, Rev. Sci. Instrum. **66**, 1584 (1995).
[40] S. Shin *et al.* (unpublished).